Accepted Manuscript

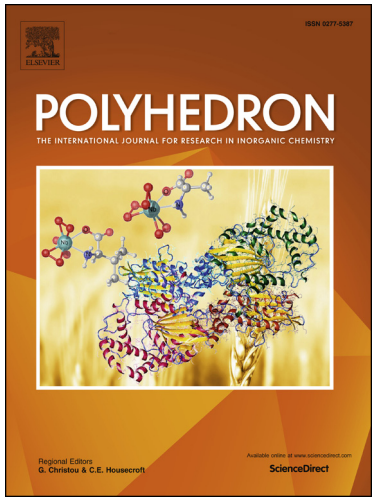

Two novel isostructural and heteroleptic Nd(III) and Dy(III)-organic frameworks constructed by 2,5-pyridinedicarboxylic acid and *in situ* generated 2-pyridinecarboxylic acid: Hydrothermal synthesis, characterization, photoluminescence properties and heterogeneous catalytic activities

Burak Ay, Emel Yildiz, İbrahim Kani

PII: S0277-5387(17)30280-2
DOI: http://dx.doi.org/10.1016/j.poly.2017.04.011
Reference: POLY 12589

To appear in: *Polyhedron*

Received Date: 15 February 2017
Accepted Date: 11 April 2017

Two novel isostructural and heteroleptic Nd(III) and Dy(III)-organic frameworks constructed by 2,5-pyridinedicarboxylic acid and *in situ* generated 2-pyridinecarboxylic acid: Hydrothermal synthesis, characterization, photoluminescence properties and heterogeneous catalytic activities

Burak Ay [a,*], Emel Yildiz [a], İbrahim Kani [b]

[a] *Çukurova University, Department of Chemistry, Arts and Science Faculty, 01330, Adana, Turkey*
[b] *Department of Chemistry, Anadolu University,26470, Eskişehir, Turkey*
Phone: +90 322 338 60 84/2442-20, Fax: +90 322 338 60 70
bay@cu.edu.tr

Abstract

The crystal structures, heterogeneous catalytic activities and photoluminescent properties of two novel three dimensional (3D) metal organic frameworks (MOFs), $[Nd(pyc)(pydc)(H_2O)]_n$ **(1)** and $[Dy(pyc)(pydc)(H_2O)]_n$ **(2)** (H_2pydc = pyridine-2,5-dicarboxylic acid, Hpyc = 2-pyridinecarboxylic acid) are presented. The synthesized complexes under hydrothermal conditions were characterized by the elemental analysis, inductively coupled plasma (ICP), fourier transform infrared (FT-IR) spectroscopy, thermogravimetric analysis (TGA), single crystal X-ray diffraction and powder X-ray diffraction (PXRD) analysis. For morphological analysis, field emission scanning electron microscopy (FESEM) and atomic force microscopy (AFM) were used. The compounds are isostructural and each Ln^{3+} (Nd(III) and Dy(III)) centers are eight-coordinated. MOFs have the distinct 3D open-framework architectures due to the presence of Hpyc ligands, which are converted from H_2pydc ligands *in-situ* decarboxylation under the hydrothermal conditions. Photoluminescence properties and thermal stabilities of the compounds have been investigated. Their heterogeneous catalytic activities have also been examined on the oxidation of the thymol (T) to thymoquinone (TQ). The structures of the MOFs were stable after three catalytic cycles. The maximum T conversion values, 40.37% and 36.45% were recorded with nearly 100% selectivities by using **1** and **2**, respectively.

Keywords: Hydrothermal synthesis, Nd(III) and Dy(III) Coordination polymers, MOFs, Decarboxylation, Heterogeneous Catalyst, Thymoquinone

1. Introduction

Metal organic frameworks (MOFs) have been received great attention because of their diversiform architectures and potential applications in the areas of molecular recognition, ion exchange, catalysis, luminescent, gas adsorption and separation processes [1-5]. MOFs containing lanthanide ions (Ln^{3+}) are the most popular class of coordination polymers. They can generate different topological structures, porous materials, unpredictable and amazing coordination polymers. Ln^{3+} ions own larger radius and higher affinity for hard donor centers and ligands with oxygen or hybrid oxygen-nitrogen atoms. Additionally, these ions with special luminescent resulting from 4f electrons, which illustrate the coordination polymers are intriguing and remarkably suitable for the development of optical devices [6]. Subcritical Water Hydrothermal Synthesis (SWHS) has become a powerful method in the synthesis of MOFs which exhibits an ideal performance on increasing the crystal growth under high temperature and pressure conditions. However, unexpected *in situ* reactions have been observed under SWHS conditions, such as formation of a sulfide-sulfide bond, the hydrolysis of carboxylate esters, cyclo addition of organic nitriles with azide and ammonia, dehydrogenative carbon-carbon coupling and decarboxylation of aromatic carboxylates [7-10]. These reactions are significantly important in synthetic chemistry. Hydro- and solvo-thermal *in situ* ligand synthesis is of great interest in coordination chemistry for the preparation of unusual coordination complexes as well as for the discovery of new organic reactions [11, 12]. This method is also provide unique medium to the synthesis of high purity catalysts used in obtain of natural drugs.

Nigella Sativa L. (black seed or black cumin) has been known as natural drug for hundred years. *Nigella Sativa L.* contains important pharmacologically active substances such as thymol (T), carvacrol, thymoquinone (TQ), dithymoquinone and thymohydroquinone [13]. TQ is the main component of the black seed, which can obtain oxidation of T by using effective homogeneous or heterogeneous catalysts. It has higher commercial value than the precursor. TQ, representing 18.4-24% of the essential oil of black seed, has many different activities. TQ has been known for its antioxidant [14], antihistamine [15], antinociceptive [16], neuropharmacological activity [17], oxidative stress [18], antimicrobial [19] and anticancer [20, 21] properties. Especially, in the past five years, it has been proven to be effective in the treatment of cancer diseases such as colon [22], pancreas [23], prostate [24] and breast [25, 26]. Some publications have been reported for the oxidation of T to TQ with heterogeneous and homogeneous catalysts [27-31]. Heterogeneous catalysts have several

advantages comparing to homogeneous catalysts, such as good dispersion of active sites, simple product isolation, easier separation from the reaction mixture, they are lesser consumption, environment-free and reusability [32-34]. Thus, the heterogeneous solid base catalysts have been recognized as potential alternatives to homogeneous catalysts.

In this study, we described the synthesis and characterization of two novel 3D open lanthanide-organic frameworks $[Nd(pyc)(pydc)(H_2O)]_n$ **(1)** and $[Dy(pyc)(pydc)(H_2O)]_n$ **(2)** containing Hpyc ligand, which was formed *in situ* from H_2pydc and lanthanum(III) salts. We observed that *in situ* hydrothermal decarboxylation reactions can occur at H_2pydc when it reacts with nitrate salts of Ln^{3+}. Interestingly, the decarboxylation of H_2pydc was observed during hydrothermal synthesis of MOFs. The results indicated that the decarboxylation occured on the 5-carboxylate group rather than the 2-carboxylate group of H_2pydc. Therefore, Hpyc takes part in the construction of both complexes as the second ligand (Scheme 2). Amazingly, the carboxylate group of Hpyc involved coordination while the pyridyl nitrogen atom could not. These novel heterogeneous catalysts with mixed ligands have been synthesized using 'one-pot' methodology by SWHS. Their crystal structures, heterogeneous catalytic activities, and photoluminescent properties of the MOFs have been examined in details.

2. Experimental

2.1. Materials and methods

$Nd(NO_3)_3.6H_2O$, $Dy(NO_3)_3.6H_2O$, H_2pydc, TQ, T, piperazine, hydrogen peroxide (30%, H_2O_2) and *tert*-Butyl hydroperoxide (~80%, TBHP) were purchased from commercial sources and used without further purification. All hydrothermal syntheses were carried out in 23 mL PTFE-lined stainless steel containers under autogenous pressure. IR spectra were recorded with KBr pellets on a Perkin-Elmer RX-1 FT-IR spectrometer in the range of 4000-400 cm^{-1}. Elemental analysis was performed on Thermo Flash 2000 CHNS. Perkin-Elmer Optima 2100DV ICP instrument was used for the quantitative lanthanide analyses. Perkin Elmer Pyris Diamond TG/DTA equipment was used for the TG analyses. Rigaku Miniflex system with CuKα radiation (λ= 1.54059 Å) was used for the PXRD studies. Solid state phosphorescence excitation and emission spectra were recorded on a Perkin-Elmer LS 55 Luminescence Spectrometer. The FESEM and AFM images were recorded using Carl Zeiss, SUPRA-55 and Nanosurf FlexAFM, respectively. A Thermo Brand chromatograph with TR5MS capillary

columns was used for the GC/MS analysis. HPLC analyses were performed on Shimadzu HPLC system equipped with a reversed phase C8 column.

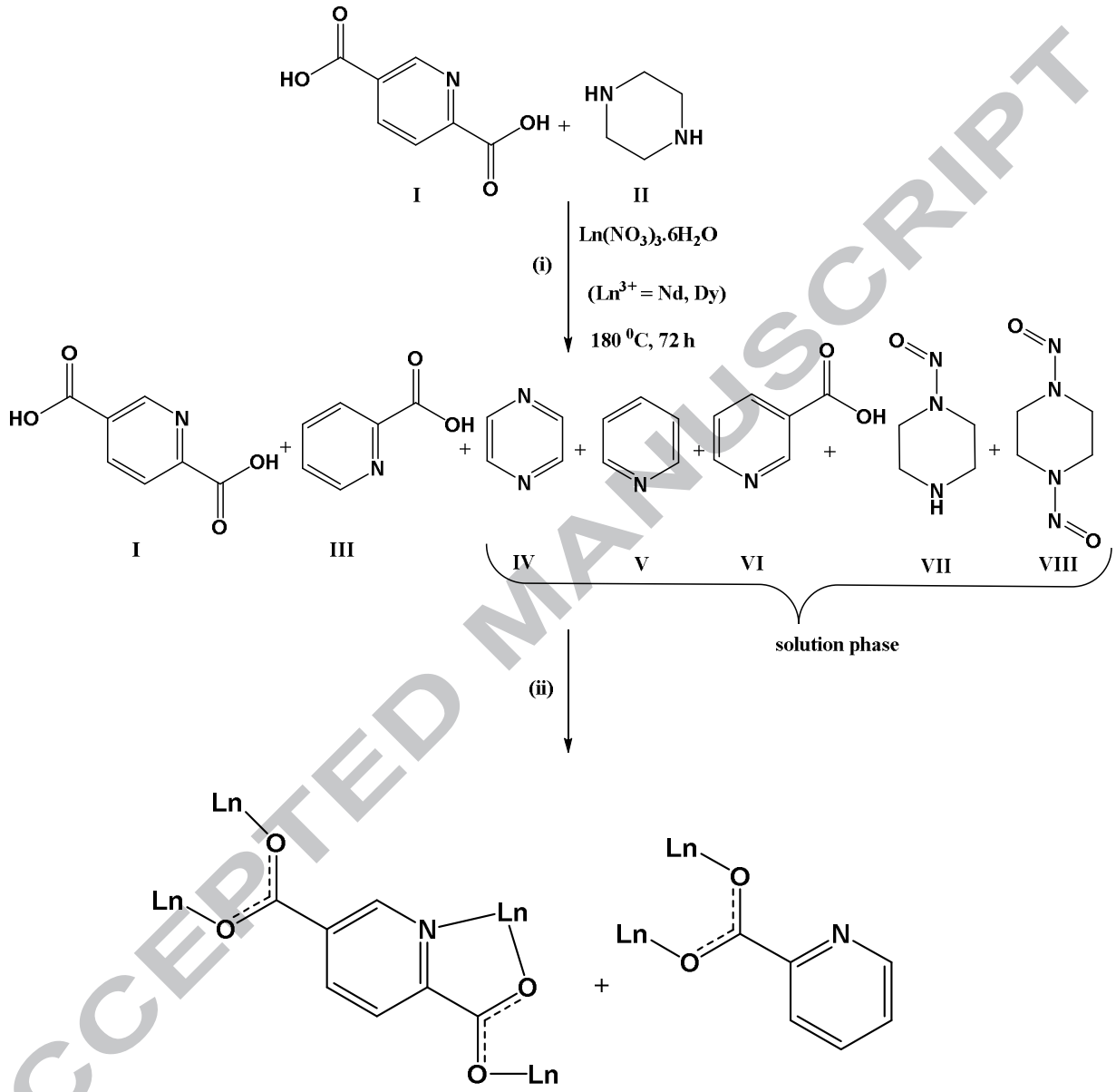

I-H_2pydc, **II-**Piperazine, **III-** Hpyc, **IV-**Pyrazine, **V-**Pyridine, **VI-**3-pyridinecarboxylic acid, **VII-**N-nitrosopiperazine, **VIII-**N-N'-dinitrosopiperazine

Scheme 1. Schematic representation of *in situ* decarboxylation and the forming new ligands in solution phase under hydrothermal conditions **(i),** and the coordination modes of the ligands with using lanthanides **(ii)**.

2.2. Synthesis of [Nd(pyc)(pydc)(H_2O)]$_n$ (1)

A solution of $Nd(NO_3)_3.6H_2O$ (0.132 g, 0.30 mmol), 2,5-pyridinedicarboxylic acid (0.150 g, 0.90 mmol), piperazine (0.026 g, 0.30 mmol), and H_2O (5 mL, 278 mmol) with the mole ratio of 1:3:1:927 was stirred before heating at 180 °C for 72 hours. The initial and final pH values were 2.20 and 3.40, respectively. The heterogeneous solution mixture was separated from the solid phase, and the crystals washed by the water, and dried at room temperature. Dark yellow crystals (Fig. 1) suitable for X-ray diffraction were isolated in 48% yield (based on Nd). Anal. Calcd. for $C_{13}H_9N_2O_7Nd$: C, 34.71; H, 2.00; N, 6.23. Found: C, 34.10; H, 2.14; N, 6.34%. The ICP analysis (%) showed that **1** contained Nd: 31.76; Calcd. For Nd: 32.10. IR data (cm^{-1}): 3487(m), 3071(m), 1661(s), 1591(s), 1481(m), 1396(s), 1363(s), 1033(m), 947(w), 820(m), 771(m), 755(m), 699(m), 590(m), 506(s), 430(w).

2.3. Synthesis of [Dy(pyc)(pydc)(H_2O)]$_n$ (2)

The preparation of MOF **2** was similar to that of MOF 1 except that $Dy(NO_3)_3.6H_2O$ (0.132 g, 0.30 mmol) was used instead of $Nd(NO_3)_3.6H_2O$. The initial and final pH values were 3.25 and 3.75, respectively. Colorless crystals (Fig. 1) suitable for X-ray diffraction were isolated in 72% yield (based on Dy). Anal. Calcd. for $C_{13}H_9N_2O_7Dy$: C, 33.35; H, 1.92; N, 5.98. Found: C, 33.77; H, 1.88; N, 6.13%. The ICP analysis (%) showed that **2** contained Dy: 33.69; Calcd. For Dy: 34.74. IR data (cm^{-1}): 3668(m), 3136(m), 1661(s), 1631(s), 1592(s), 1560(s), 1488(m), 1407(s), 1369(s), 1287(w), 1160(w), 945(m), 832(m), 761(m), 693(m), 573(w), 524(m), 437(w).

2.4. X-ray structure determination

The crystallographic data collection for **1** and **2** were collected with a Bruker AXS APEX CCD diffractometer equipped with a rotation anode at 296(2) K using graphite monocromated Mo Kα radiation (λ = 0.71073 Å). Diffraction data were collected over the full sphere and were corrected for absorption. A Bruker SMART [35] program package was used for the data reduction. Crystal data and structure refinement for the MOFs are summarized in Table 1. Structure solution was found with the SHELXS-97 [36] package using the direct methods, and refined SHELXL-97 [37] against F^2 using first isotropic and later anisotropic thermal

parameters for all nonhydrogen atoms. Hydrogen atoms were added to the structure model on calculated positions. Geometric calculations were performed with Platon [38].

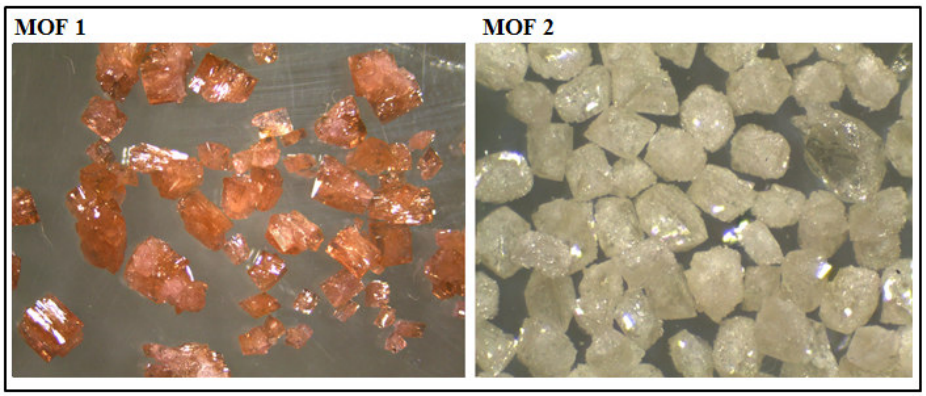

Figure 1. High definiton microscope views of the synthesized MOFs.

3. Results and discussion

3.1. *Descriptions of crystal structures of the catalysts*

Single-crystal X-ray diffraction studies revealed that **1** and **2** are isostructural, whose crystals fall in the same centrosymmetric space group ($P2_1/c$). The symmetric and asymmetric X-ray crystal structures of the Nd(III) and Dy(III) complexes are shown in Fig. 2. The crystal data and structure refinement for the MOFs are given in Table 1. The selected bond lengths (Å) and bond angles (°) of **1** and **2** are given in Table S1 and S2. For the convenience of depiction, the structure of **1** is described as a representative example in detail here. MOFs are crystallizes in the monoclinic system, space group $P2_1/c$. Each asymmetric unit of Ln^{3+} complexes contains one metal atom, one H_2pydc, one Hpyc and one water molecule (Fig. 3).

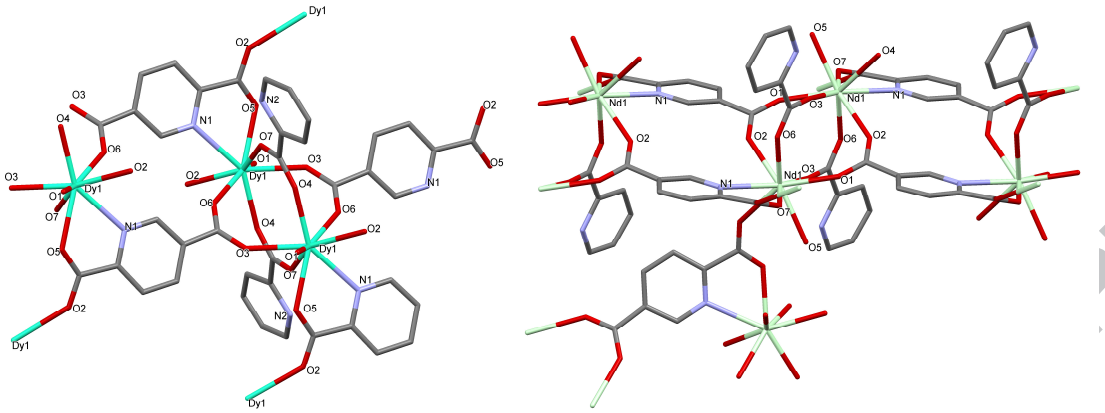

Figure 2. Molecular structure of **1** (a), and **2** (b). All hydrogen atoms are omitted for the clarity.

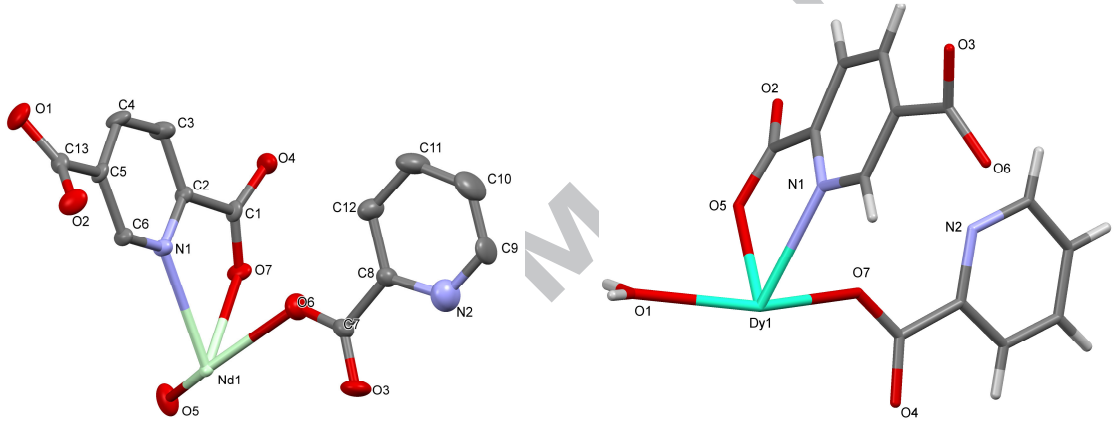

Figure 3. Asymmetric unit of **1** and **2**.

Figure 5(b) shows that two Hpyc and two H_2pydc carboxylate groups function as a bidentate bridge and connect two Nd(III) ions to form a dimeric molecule with a Nd1⋯Nd1 Å separation of 4.532 Å. Within the binuclear unit the pydc ligands chelates exclusively to a single Ln site through the nitrogen donor, and one carboxylate terminus while the second carboxylate group of same $pydc^{2-}$ ligand bridges two Ln centers of dimer. Metal to metal distance between two building binuclear units, $[Ln_2(H_2pydc)_4(Hpyc)_2(H_2O)]_n$ linked through two $pydc^{2-}$ ligands, is 6.843 Å. Moreover, $pydc^{2-}$ ligands act as a bridge to link different Ln(III) ions of adjacent chains, resulting in three-dimensional network structure (Fig. 5a). As shown in Fig. 5b, in 3D structure of 1, the distances among five adjacent Nd(III) ions are 4.532, 6.260, 7.952, 9.353, 10.833 and 11.663 Å . Each Ln(III) ion is further bonded to one chelated pydc through N and O atoms, one carboxylato oxygen of neighboring pydc, and one aqua molecule.

Table 1

Crystal data and structure refinement for **1** and **2**.

Code	**1**	**2**
Empirical formula	$C_{13}H_9N_2O_7Nd$	$C_{13}H_9N_2O_7Dy$
Formula weight	450.47	467.72
Temperature	296(2) K	296(2) K
Wavelength	0.71073 Å	0.71073 Å
Crystal system	Monoclinic	Monoclinic
Crystal size	0.31 x 0.18 x 0.15 mm	0.21 x 0.38 x 0.19 mm
Space group	$P2_1/c$	$P2_1/c$
Unit cell dimensions	a = 9.353(3)Å α = 90°	a = 9.1977(11) Å α = 90°
	b = 14.316(5) Å β = 95.413(13)°	b = 14.1014(17) Å β = 95.983(4)°
	c = 10.556(5)Å γ = 90°	c = 10.4690(13) Å γ = 90°
Volume	1407.2(8) $Å^3$	1350.5(3) $Å^3$
Z	4	4
Density (calculated)	2.126 Mg/cm^3	2.300 Mg/cm^3
Absorption coefficient	3.730 mm^{-1}	5.575 mm^{-1}
F(000)	872	892
Theta range for data collection	2.19 to 28.68°	2.23 to 28.31°
Index ranges	-11<=h<=12, -19<=k<=19, -13<=l<=13	-12<=h<=11, -18<=k<=18, -13<=l<=13
Reflections collected	59287	48051
Unique reflections	3441 [R(int) = 0.0340]	3317 [R(int) = 0.0267]
Max. and min. transmission	0.6046 and 0.3910	0.6046 and 0.3910
Data / restraints / parameters	3441 / 0 / 216	3317 / 1 / 216
Goodness-of-fit on F^2	1.014	1.024
Final R indices [I>2σ(I)]	R1 = 0.0226, wR2 = 0.0698	R1 = 0.0160, wR2 = 0.0406
R indices (all data)	R1 = 0.0238, wR2 = 0.0708	R1 = 0.0166, wR2 = 0.0408
Largest diff. peak and hole	0.889 and -1.071 e.$Å^{-3}$	0.785 and -0.807 e.$Å^{-3}$

The Ln^{3+} ion in the complexes is eight-coordinated and consists of six O-atoms and one N-atom from pyridine carboxylate ligands, and one O-atom from water. The coordination geometry of the Ln^{3+} ions can be described as a distorted square-antiprism (Fig. 4), with atoms O3, O4, O6 and O7 (for **2**) / O1, O2, O3 and O6 (for **1**) forming the upper and O1, O2, O5 and N1 (for **2**) / O4, O5, O7 and N1 (for **1**) forming the lower plane. The mean plane angle between upper and lower squares is 5.579^{o} and 6.790^{o} for **1** and **2** respectively.

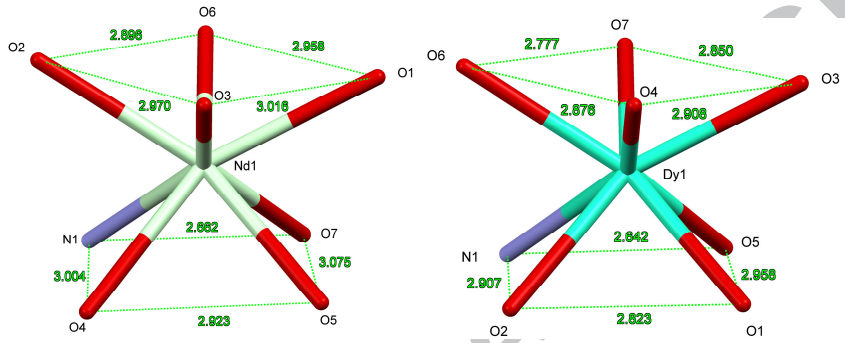

Figure 4. Square antiprism coordination geometry of **1** and **2**.

The 2,5-pydc groups are coordinated to the Ln^{3+} ion and can be classified into three different coordination modes (Fig. 6): Pyridine and carboxylate group N–C–O are in a chelating mode, in which nitrogen of pyridine ring and one of the oxygen of terminus carboxylato group coordinate to the same Ln^{3+} ion, the second oxygen atom of carboxylato group coordinate to neighboring Ln^{3+}, the second carboxylato group (O–C–O) of same ligand is in a bidentate mode, in which two O atoms coordinate to two different Ln^{3+} ions to form a dimer. The 2-pydc group is coordinated to the lanthanide ions with only one type of coordination mode in which two oxygens of carboxylato group coordinate to two different center in dimeric unit through bidentate bridging mode.

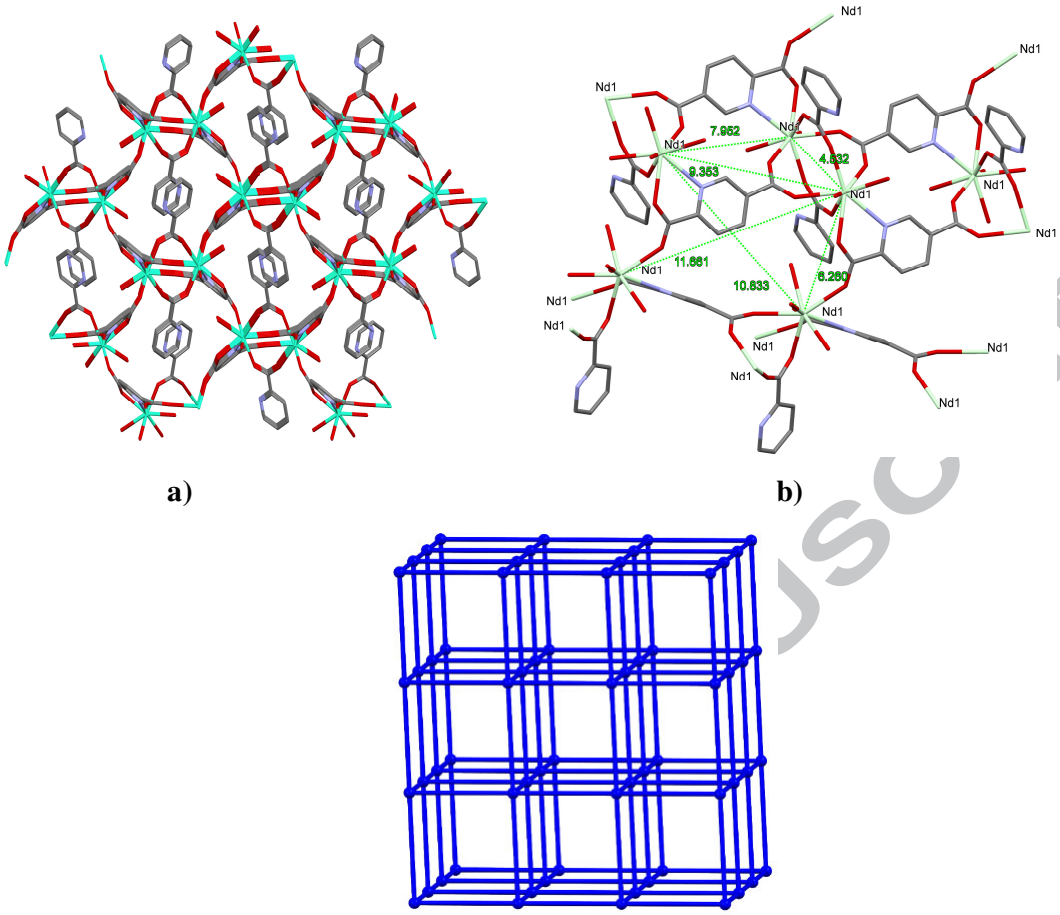

Figure 5. a) 3D structure of **1. b)** Nd-Nd distances in the structure of **1**. **c)** A schematic view of the uninodal 6-connected 3D framework of complex **1** and **2.**

The average bond lengths of Nd–$O_{(carboxyl)}$ and Dy–$O_{(carboxyl)}$ bonds of the present complexes are 2.35(3) and 2.326 (2) Å, and the O–Nd–O and O–Dy–O bond angles lie in the range 62.15(8)–149.6(9) ° and 63.91-148.3 (7) °, respectively (Table S1-S2). A comparative study shows that the average Dy–O and Nd–O bond lengths are consistent with reported Dy(III) and Nd(III) complexes [39-42]. The bond length for the oxygen atom of the water molecule to Nd and Dy ions are 2.457 (3) Å and 2.369 (2) Å, respectively. In the crystal structure, some important strong intra- and inter-molecular hydrogen bondings were observed among the water molecule, pydc and pyc ligands. The hydrogen bond details are presented in Table S3. Topological analysis showed that complex **1** and **2** have the same uninodal 6-connected 3D framework and display pcu topology with the point symbol of (412.63) (Fig. 5c) [42-a].

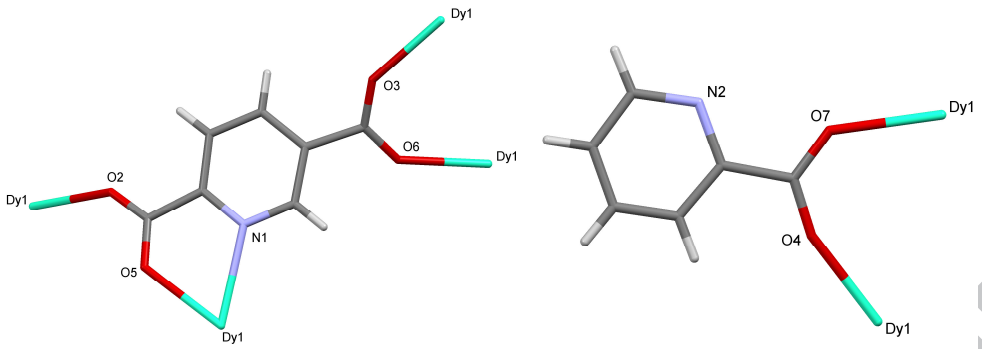

Figure 6. The coordination modes of pydc and pyc for **1**.

3.2. In situ hydrothermal decarboxylation and formation

GC-MS analysis was performed for the solution phase to understand new ligands formation, and the possible reaction mechanism of *in situ* decarboxylation under hydrothermal conditions. Interestingly, five new ligands, namely 3-pyridinecarboxylic acid, N-nitrosopiperazine, N,N'-dinitrosopiperazine, pyrazine and pyridine, formation were observed in the solution phase (**Scheme 1-i**). This result supported to decarboxylation reaction, and formation of new ligands (Fig. S1). Nitroso groups came from the nitrate salts of the lanthanide metals, and linked to only piperazine ligands in two different ways under hydrothermal conditions. The decarboxylation was observed at 5-carboxylate group and formed Hpyc in the presence of $Nd(NO_3)_3.6H_2O$ and $Dy(NO_3)_3.6H_2O$ at 180 °C. As shown in **Scheme 1-ii**, H_2pydc and Hpyc ligands coordinated to the lanthanide atoms in different coordination modes. Zhao et al. reported the *in situ* decarboxylation mechanism at high temperature and pressure for the deprotonating of carboxylic acids. According to the Arrhenius equation, $dlnk/dT = E/RT^2$, the reaction rate accelerates with the increase of temperature under confined compression [43]. Lanthanide salt species have an impact on *in situ* decarboxylation reactions as well as temperature and pressure values. For instance, the H_2pydc do not lose its carboxyl group in the presence of chloride salts of lanthanide at low reaction temperatures. In addition, if the same experiment is performed without metal salt in the equal conditions, neither decarboxylation nor new ligand formations observe in the solution phase by GC-MS analysis. Consequently, the nitrate salts of the lanthanides have a catalytic role in decarboxylation and formation of new ligands at high temperature under subcritical water conditions.

3.3. FT-IR spectra

The FT-IR spectra of the free H_2pydc and the synthesized MOFs are shown in Figs. S2-S4. Their absorption bands are assigned to the υ(O-H) stretching vibrations of coordinated water molecules in unit cell in the ranges of 3680-3300 cm^{-1} [44, 45]. The carboxyl band of the ligand is found at 1730 cm^{-1}. The absence of this band indicates that H_2pydc are completely deprotonated in the form of $pydc^{2-}$ anions upon reaction with the metal ions. For **1**, the two strong bands are at 1661 and 1396 cm^{-1} corresponding to the stretching vibrations of asymmetric and symmetric carboxyl groups. For **2**, these bands are observed at 1631 and 1407 cm^{-1}, respectively [46, 47]. Other important supporting evidence is metal nitrogen/oxygen absorption band to ensure the coordination. The Ln-N and Ln-O stretching vibrations were observed between 400 and 550 cm^{-1}. The medium bands at 506 and 430 cm^{-1} may be ascribed to υ(Nd-N) [48] and υ(Nd-O) [49]. The new bands, having medium intensities at 524 and 437 cm^{-1}, can be assigned to the υ(Dy-N) [50] and υ(Dy-O) [51] stretching vibrations. These absorption values are absent in the infrared spectra of the ligand. The obtained results are in agreement with the data from the single crystal X-ray analysis.

3.4. Thermal analysis and PXRD patterns

To determine thermal stability of the complexes, MOFs crystals were selected under an optical microscope. The similar thermal curves were obtained due to the isostructural nature of the compounds (Fig. 7). Their thermogravimetric (TG) analysis was performed in the temperature range from 50 to 800 °C under N_2 atmosphere with a heating rate of 10 ºC.min^{-1}. TG/DTG analysis supported the single crystal X-ray results of the MOFs (Figs. S5-S6). The compounds are thermally stable up to ~200 °C. Above this temperature, the two TG curves of compounds exhibited two main steps of weight loss. The TG curve of **1** showed the first weight loss of 4.20% in the temperature range 201 to 317 °C, corresponding to the loss of one coordinated water molecule per formula unit (Calcd. 4.00%). The second significant weight loss of 61.79% corresponds to the decomposition of H_2pydc and Hpyc ligands in the framework in the temperature range of 340 to 563 °C, (Calcd. 63.90%). The residual weight of 33.98% is attributed to the final product of Nd_2O_3 (Calcd. 32.09%). The TG plot of **2** also showed the weight loss of 3.36% in the first stage between 221 and 333 °C, attributable to the loss of a coordinating water molecule in formula unit (Calcd. 3.85%). The next weight loss of 59.04% corresponds to the decomposition of H_2pydc and Hpyc ligands in the framework in

the temperature range of 409-646 °C, (Calcd. 61.40%). The remaining weight of 33.98% corresponds to Dy_2O_3, which is slightly greater than the calculated value of 34.74% because of uncompleted decomposition.

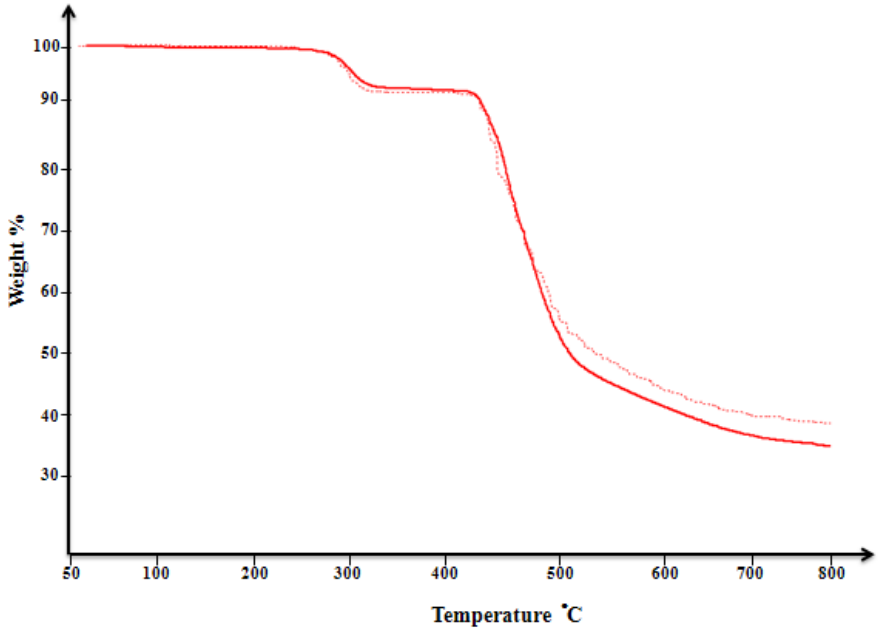

Figure 7. Thermogravimetric curves of **1** (solid line) and **2** (dotted line).

To determine the phase purities of the synthesized MOFs, the PXRD analysis were performed at room temperature. Simulated patterns were obtained by using the single crystal data and diffraction-crystal module of the Mercury (Hg) program. The experimental and simulated XRD patterns of the MOFs from single-crystal X-ray data were shown in Fig. S7. These patterns were compared with each other in terms of peak positions. The PXRD patterns of the compounds are in good agreement with each other on the basis of the single crystal structures. The compounds have been successfully obtained as pure crystalline phases, and have high purities. Their high resolution microscope images support these results (Fig. 1).

3.5. Morphologies of the MOFs

The surface morphologies and microstructures of the obtained MOFs were performed by using FESEM and AFM analyses. These techniques were significantly helpful to determine the particle sizes and identify the distinct morphologies of the MOFs. Although the MOFs were synthesized with the H_2pydc and Hpyc ligands, their morphologies were found in different shapes and sizes vary from 1 to 100 μm due to the using Nd(III) and Dy(III) metals.

The images of **1** and **2** show smart look with thick shaped structure or stratified, which indicate crystalline nature. The stratified shape structures are due to the aggregation of a great number of monomers leading to the polymerization.

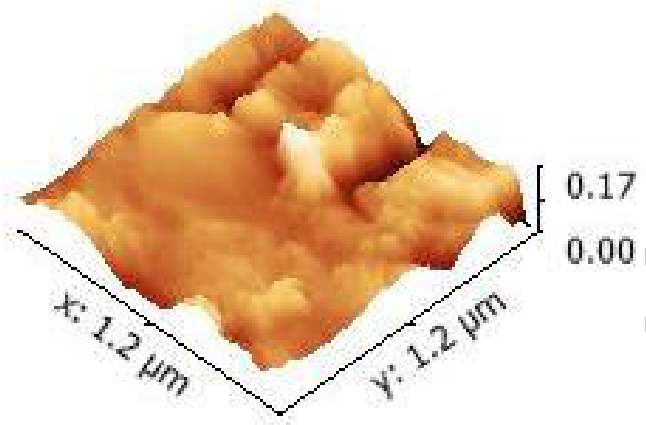

(a)

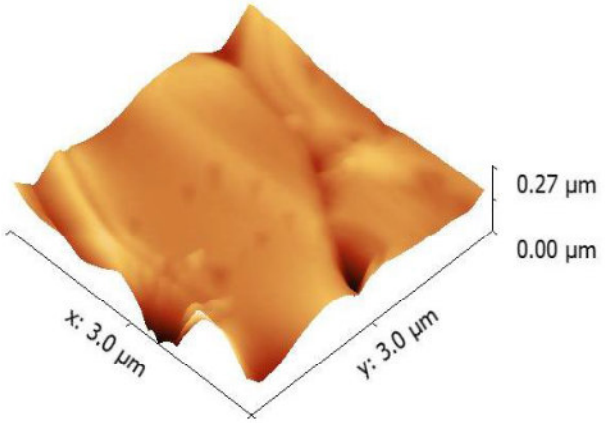

(b)

Figure 8. AFM images of **1** (a) and **2** (b).

The FESEM images supported that the synthesized MOFs were in polymeric form. The 3D topographic images of the MOFs were characterized by using AFM, as shown in Figs. 8-9. The topographies determined in 1.2 × 1.2 μm^2 for Nd(III) and 3.0 × 3.0 μm^2 for Dy(III) reveal bumpy areas. In addition, **1** (roughness 22.21 nm) showed a higher level of roughness compared to **2** (roughness 15.68 nm). These values supported that the surfaces are uniform and compact [52]. The image of **2** is found to be more relatively smooth and homogeneous compared to **1**. The image of **2** showed much less smooth with sharp and rough structure.

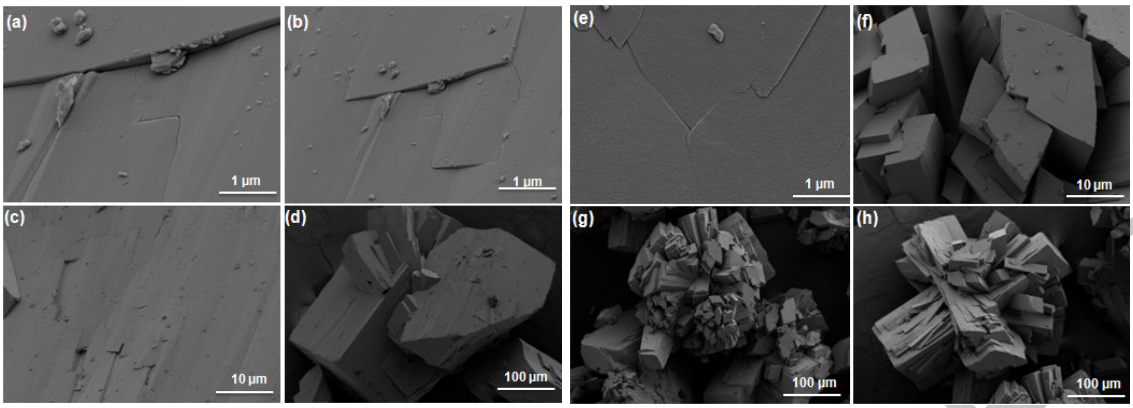

Figure 9. FESEM images of single crystals of **1** (a-d) and **2** (e-h).

3.6. Photoluminescence properties

The photoluminescence properties of free H_2pydc, and the synthesized MOFs were examined in the solid state at room temperature, as shown in Fig. 10. The synthesized MOFs exhibited similar wide bands ranging from 500 to 600 nm. It is worth mentioning that we could not see any characteristic emissions of Nd^{3+} and Dy^{3+} ions in the emission spectra of the complexes. To understand the nature of the photoluminescence properties of the MOFs, the emission spectrum of free ligand was measured under the same conditions. It was obtained three primary emission bands in the regions of 200-300 nm (λ_{ex}: 190 nm) [53]. Compared to the H_2pydc, the emission broad band of **1** mainly ranges from 560 to 600 nm with the maximum wavelengths at 580 nm under excitation of 302 nm. For **2**, the emission wide band ranges from 590 to 640 nm with the maximum wavelengths at 608 nm under excitation of 302 nm. The photoluminescence emission bands are red shifted in the MOFs. The red shift is presumably related to the intraligand luminescence emission [54]. Considering the strong emission peaks at 580 nm for **1**, and 608 nm for **2**, which were different from the emission band of the free ligand greatly. The lower energy band would be assigned to the ligand-to-metal charge transfer (LMCT) [55, 56], and observed emission values of the complexes are supported to the coordinated ligands to Nd^{3+} and Dy^{3+} ions.

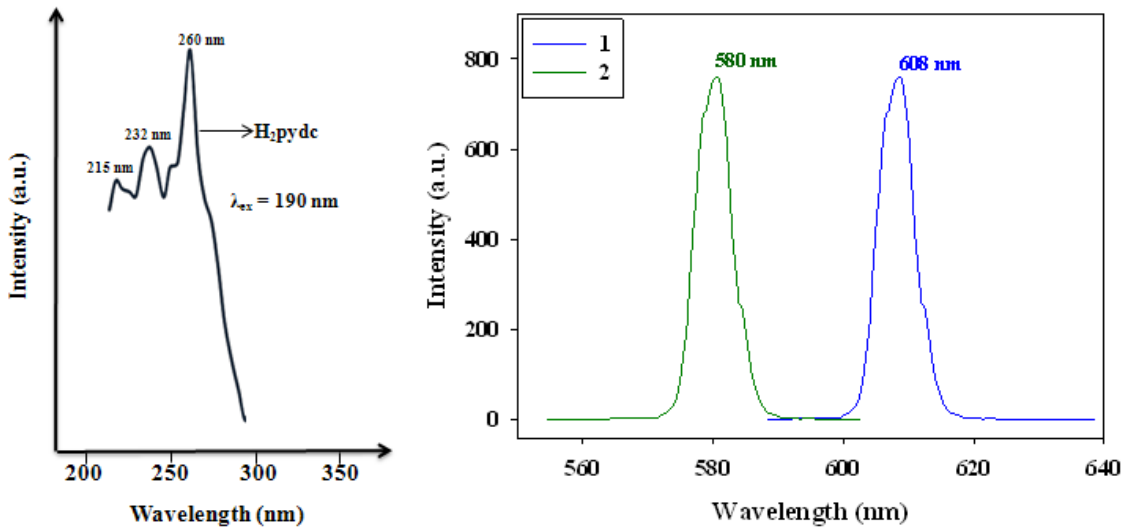

Figure 10. Solid state photoluminescence spectra of H_2pydc and MOFs at room temperature.

3.7. *Catalytic activity studies*

Although homogeneous catalysts have higher selectivity, they cannot be easily recovered from the reaction medium by filtration like heterogeneous catalysts. Catalyst recovery is a very important property for the industrial processes. Heterogeneous catalysts are superior to homogeneous catalysts due to this characteristic feature. Cheap and environmentally friendly oxidant agents namely H_2O_2 and TBHP have mostly been used as oxidant agents in the examination of the catalytic activities of MOFs towards oxidation reactions in a heterogeneous medium. H_2O_2 and TBHP reagents were used as oxidant agents for the catalytic reactions in acetonitrile. All reactions were performed in the temperature of 60 °C. The catalytic activity studies were performed according to the reference [57]. The obtained T conversion values (%) in different conditions are given in Table 2. The characterization of the TQ was performed by GC/MS (Fig. S8). The catalytic performance of the catalysts was determined by HPLC analysis. The retention times of the T and oxidation product, TQ were detected at 254 nm by HPLC before the catalytic studies (Figs. S9-S10). The clear thing is T cannot be oxidized to TQ without catalyst but only trace amount of product (Fig. S11). Whereas, Using **1** and **2**, T significantly oxidized to TQ (Figs. S12-S13). TQ is obtained in trace amounts in the absence of catalyst (**see Scheme 2**). The conversion values were plotted as a function of temperature in 60 °C for the determination of their catalytic activities. According to HPLC analysis, maximum T conversion values were 40.37% with H_2O_2, and 32.71% with TBHP by using **1**. On the other hand, 36.45% with H_2O_2 and 22.05% with TBHP

were obtained in the medium of **2**. It was not observed any by products in all the HPLC chromatograms, so their selectivities were approximately 100% (Figs. S14-S17). Other variables such as amount of the catalysts, type of the oxidant agents and reaction times are shown in Table 4. The activities of the MOFs were optimized with 0.15 g of complex using H_2O_2 and TBHP as oxidants at 60 °C. In both oxidant agents, T conversion values were obtained maximum rate when the reaction time and MOFs amounts increased. To determine the whether catalytic effect of the ligand and metal salts or not, the same catalytic reaction medium were prepared. It was not observed any product in the HPLC chromatogram by using only ligand. Trace amounts of TQ were obtained using both solely Nd(III) and Dy(III) salts (Figs. S18-S20) for the same aim. These results showed that ligand and lanthanide salts were not showed any significant catalytic activities in the oxidation of T to TQ. At the end of the catalytic studies, it was not observed any by-product except main oxidation product by using **1** and **2** as catalysts, and oxidant agents. The maximum T conversion values, 40.37% and 36.45% were recorded with nearly 100% selectivities by using **1** and **2**, respectively. As it seen from the PXRD results and the high definition microscope views, the MOFs have high purities and crystallinity properties.

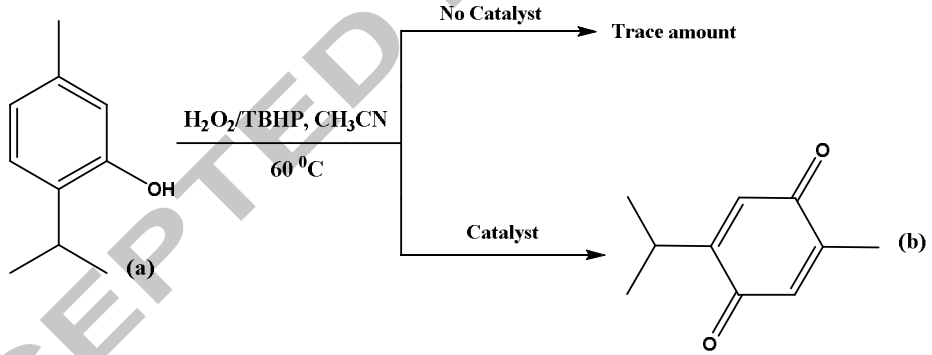

Scheme 2. Oxidation of T **(a)** to TQ **(b)** using catalyst and without catalyst.

3.8. Separation and reusability of the MOFs

Reusability is one of the important properties for the heterogeneous catalysts. They can be recycled easily from the reaction medium using convenient solvents. To examine the reusability of the MOFs, four sequential reactions were performed for 0.15 g MOFs using hydrogen peroxide as an oxidant agent for 24 hours at 60 °C. After every reuse, the catalysts were separated from the reaction mixture, filtered off, and washed with methanol (10 mL),

acetone (10 mL), and then dried at room temperature. The conversion values remained comparable worth after three tests. These results support the reusability of the catalysts without any significant loss of activity (Table S4), but these values decreased in the fourth tests. The obtained results showed that the MOFs have long usability for the oxidation of T to TQ (Fig. 11). The MOFs contents of the filtrates were determined by ICP analysis after the separation of the catalysts by filtration. At the end of the four runs, only 1.8% of **1** and 1.5% of **2** were lost into the solution during the reusability reactions.

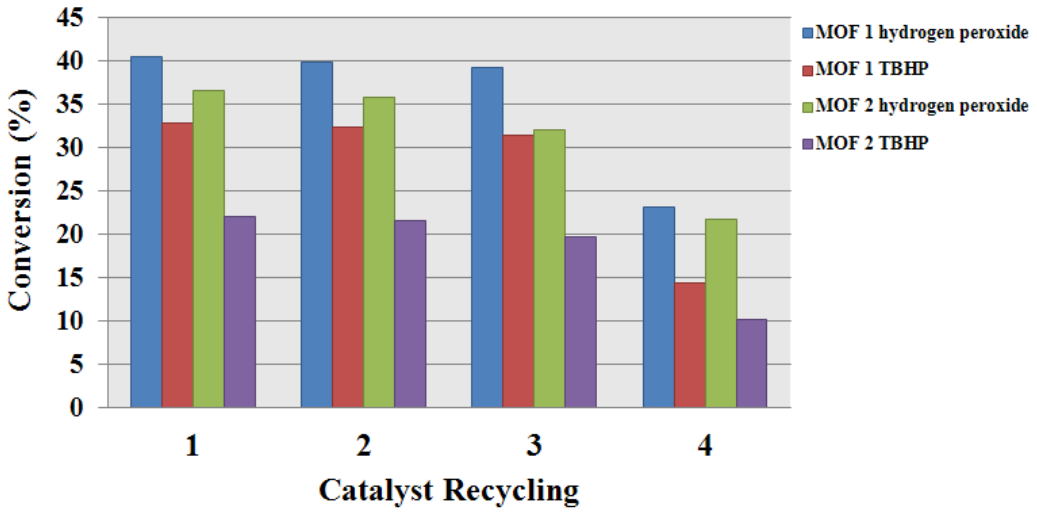

Figure 11. The effects of oxidants on the oxidation reaction for the MOFs catalytic system.

Table 2

% T conversion values under different reaction conditions.

H_2O_2				TBHP			
Catalyst	*Catalyst Amount (g)*	*Reaction Time (hour)*	*T Conversion (%)*	*Catalyst*	*Catalyst Amount (g)*	*Reaction Time (hour)*	*T Conversion (%)*
		3	2.63			3	3.67
		6	5.70			6	5.91
	0.05	9	9.07		0.05	9	10.37
		12	10.34			12	15.56
		24	12.17			24	21.13
		3	3.22			3	4.60
		6	6.17			6	7.67
1	0.10	9	13.07	**1**	0.10	9	12.27
		12	18.46			12	17.35
		24	24.50			24	22.90
		3	9.24			3	5.07
		6	18.66			6	8.33
	0.15	9	25.50		0.15	9	16.11
		12	29.31			12	24.08
		24	**40.37**			24	**32.71**
		3	1.64			3	1.66
		6	4.16			6	2.70
	0.05	9	5.29		0.05	9	3.55
		12	7.58			12	6.06
		24	9.14			24	7.89
		3	3.22			3	3.33
		6	7.19			6	5.70
2	0.10	9	10.58	**2**	0.10	9	8.64
		12	14.17			12	11.28
		24	18.23			24	14.44
		3	6.07			3	5.17
		6	11.80			6	7.27
	0.15	9	19.91		0.15	9	11.37
		12	28.67			12	16.57
		24	**36.45**			24	**22.05**

(Temperature: 60 °C; Catalyst: $[Nd(pyc)(pydc)(H_2O)]_n$ **(1)** ; $[Dy(pyc)(pydc)(H_2O)]_n$ **(2)** ; Solvent: Acetonitrile).

In order to evaluate the efficiency of the present catalysts, we have compared the obtained results of the oxidation of the T with those of other catalysts and shown in the Table 3. Although Mn(TDCPP)Cl and FePor catalysts show high selectivity and good T conversion, they are homogeneous catalysts and can only be used once. Others, $[Mn^{III}(H_2O)BW_{11}O_{39}]^{6-}$ shows 35-40% conversion but four major oxidation products, 2-isopropyl-5-methyl-1,4-benzoquinone, 2-hydroxy-3-isopropyl-6-methyl-1,4-benzoquinone, 2-hydroxy-6-isopropyl-3-methyl-1,4-benzoquinone and 4-hydroxy-3-isopropyl-6-methyl-1,2-benzoquinone, are found. FePcTS shows 99% conversion, whereas three major products TQ and two different polymers occur. As a heterogeneous catalyst, MnTBzPyP shows 100% selectivity and less than 18% conversion. The synthesized heterogeneous catalysts show similar selectivity, which are higher conversion values than the MnTBzPyP catalyst. Clearly, the present catalysts also give higher yield than the previous heterogeneous catalytic studies. Their most important advantage over other catalysts is that they can be used three times for the oxidation of T to TQ.

Table 3

Comparison of the results obtained for the oxidation of the T with other catalysts.

Catalyst	Catalyst Type	Oxidant	T (°C)	Selectivity (%)	% T	Ref.
Mn(TDCPP)Cl	Homogeneous	H_2O_2	RT	98.9	-	[27]
MnTBzPyP	Heterogeneous	H_2O_2	RT	100	<18	[28]
$[Mn^{III}(H_2O)BW_{11}O_{39}]^{6-}$	Homogeneous	H_2O_2	BP	-	35-40	[29]
FePcTS	Homogeneous	$KHSO_5$	RT	18-31	99	[30]
FePor	Homogeneous	$KHSO_5$	RT	-	47.6	[31]
MOF 1	Heterogeneous	H_2O_2	60	100	40.37	TW
MOF 1	Heterogeneous	TBHP	60	100	32.71	TW
MOF 2	Heterogeneous	H_2O_2	60	100	36.45	TW
MOF 2	Heterogeneous	TBHP	60	100	22.05	TW

RT: Room temperature, BP: Boiling point, TW: This work

4. Conclusions

In conclusion, we have successfully synthesized two novel heterogeneous MOFs based on pyridine-2,5-dicarboxylic acid, and *in situ* formed 2-pyridinecarboxylic acid under hydrothermal conditions. The resulting decarboxylated ligand, 2-pyridinecarboxylic acid, is

observed as the second organic linker in the frameworks. Isostructural Nd(III) and Dy(III) complexes are eight-coordinated with the oxygen atoms from pyc^-, oxygen and nitrogen atoms from $pydc^{2-}$, and water molecule. When the pyc^- acts as a mono dentate ligand from the O-donor atom, the $pydc^{2-}$ is coordinated via two oxygen and one nitrogen atoms, acting as a tridentate ligand.

The heterogeneous catalysts showed high selectivity (100%) in the oxidation of T to TQ. It was not observed any by-product in all HPLC chromatograms. The catalysts can be used for three cycles and they are convenient heterogeneous catalysts for the oxidation of T to TQ. Moreover, their photoluminescent spectra show that **1** and **2** have potential luminescent properties at the maximum emissions at 580 and 608 nm, respectively.

Acknowledgements

The authors gratefully acknowledge financial support from the Research Unit of Çukurova University (Grant No. FEF2013D5), and the Medicinal Plants and Medicine Research Centre of Anadolu University, Eskişehir, Turkey, for the use of X-ray Diffractometer.

Appendix A. Supplementary material

CCDC 1456508 and 1456507 contains the supplementary crystallographic data for complexes **1** and **2**, respectively. These data can be obtained free of charge via http://www.ccdc.cam.ac.uk/conts/retrieving.html, or from the Cambridge Crystallographic Data Centre, 12 Union Road, Cambridge CB2 1EZ, UK; fax: (+44) 1223-336-033; or e-mail: deposit@ccdc.cam.ac.uk.

References

[1] L.-F. Yuan, J. Li, R.-P. Liu, B. Liu, H. Guo, F.-X. Zhang, Inorg. Chim. Acta 404 (2013) 197-200.
[2] N. Pawlak, G. Oczko, P. Starynowicz, Polyhedron, 101 (2015) 152-159.
[3] M.H. Alkordi, Y. Liu, R.W. Larsen, J.F. Eubank, M. Eddaoudi, J. Am. Chem. Soc. 130 (2008) 12639-12641.
[4] D. Jiang, T. Mallat, F. Krumeich, A. Baiker, J. Catal. 257 (2008) 390-395.
[5] J. Lee, O.K. Farha, J. Roberts, K.A. Scheidt, S.T. Nguyen, J.T. Hupp, Chem. Soc. Rev. 38 (2009) 1450.
[6] L. Yang, L. Liu, L. Wu, Z. Xu, L. Wang, Dyes Pigments, 111 (2014) 176-184.
[7] J.-C. Jin, W.-Q. Tong, A.-Y. Fu, C.-G. Xie, W.-G. Chang, J. Wu, G.-N. Xu, Y.-N. Zhang,

J. Li, Y. Li, P.-Q. Yang, J. Solid State Chem. 225 (2015) 216-221.
[8] J.-Y. Hu, J. Wen, X.-G. Yang, M. Chen, C.-S. Liu, Inorg. Chem. Commun. 33 (2013) 25-28.
[9] Q. Wang, Y. Fan, T. Song, J. Xu, J. Wang, J. Chai, Y. Liu, L. Wang, L. Zhang, Inorg. Chim. Acta 438 (2015) 128-134.
[10] C.-M. Liu, D.-Q. Zhang, D.-B. Zhu, Inorg. Chem. Commun. 11 (2008) 903-906.
[11] X.-M. Zhang, Coordin. Chem. Rev. 249 (2005) 1201-1219.
[12] X.-M. Chen, M.-L. Tong, Accounts Chem. Res. 40 (2007) 162-170.
[13] B. Ay, G. Yağ, E. Yildiz, A.L. Rheingold, Polyhedron, 88 (2015) 164-169.
[14] M. Ismail, G. Al-Naqeep, K.W. Chan, Free Radical Bio. Med. 48 (2010) 664-672.
[15] M. Toghyani, M. Toghyani, A. Gheisari, G. Ghalamkari, M. Mohammadrezaei, Livest. Sci. 129 (2010) 173-178.
[16] M.A. Abdel-Fattah, M. Kinzo, W. Hiroshi, Eur. J. Pharmacol. 400 (2000) 89-97.
[17] T.B. Al-Naggar, M.P. Gómez-Serranillos, M.E. Carretero, A.M. Villar, J. Ethnopharmacol. 88 (2003) 63-68.
[18] M.N. Nagi, H.A. Almakki, M.M. Sayed-Ahmed, A.M. Al-Bekairi, Food Chem. Toxicol. 48 (2010) 2361-2365.
[19] B. Ay, E. Yildiz, J.D. Protasiewicz, A.L. Rheingold, Inorg. Chim. Acta 399 (2013) 208-213.
[20] M.L. Salem, Int. Immunopharmacol. 5 (2005) 1749-1770.
[21] B. Ay, E. Yildiz, S. Jones, J. Zubieta, Inorg. Chim. Acta 387 (2012) 15-19.
[22] H. Jrah-Harzallah, S. Ben-Hadj-Khalifa, A. Maloul, R. El-Ghali, T. Mahjoub, J. Funct. Foods, 5 (2013) 1310-1316.
[23] M. Yusufi, S. Banerjee, M. Mohammad, S. Khatal, K. Venkateswara Swamy, E.M. Khan, A. Aboukameel, F.H. Sarkar, S. Padhye, Bioorg. Med. Chem. Lett. 23 (2013) 3101-3104.
[24] C.C. Woo, A.P. Kumar, G. Sethi, K.H.B. Tan, Biochem. Pharmacol. 83 (2012) 443-451.
[25] S. Rajput, B.N.P. Kumar, K.K. Dey, I. Pal, A. Parekh, M. Mandal, Life Sci. 93 (2013) 783-790.
[26] K.M. Sutton, C.D. Doucette, D.W. Hoskin, Biochem. Bioph. Res. Co. 426 (2012) 421-426.
[27] R.R.L. Martins, M.G.P.M.S. Neves, A.J.D. Silvestre, A.M.S. Silva, J.A.S. Cavaleiro, J. Mol. Catal. A-Chem. 137 (1999) 41-47.
[28] F.C. Skrobot, A.A. Valente, G. Neves, I. Rosa, J. Rocha, J.A.S. Cavaleiro, J. Mol. Catal. A-Chem. 201 (2003) 211-222.
[29] I.C.M.S. Santos, M.M.Q. Simões, M.M.M.S. Pereira, R.R.L. Martins, M.G.P.M.S. Neves, J.A.S. Cavaleiro, A.M.V. Cavaleiro, J. Mol. Catal. A-Chem. 195 (2003) 253-262.
[30] T. Günay, Y. Çimen, R.B. Karabacak, H. Türk, Catal. Lett. 146 (2016) 2306-2312.
[31] M. Milos, Appl. Cat. A-Gen. 216 (2001) 157-161.
[32] K. Aghapoor, L. Ebadi-Nia, F. Mohsenzadeh, M. Mohebi Morad, Y. Balavar, H.R. Darabi, J. Organomet. Chem. 708-709 (2012) 25-30.
[33] C. Rossy, J. Majimel, M.T. Delapierre, E. Fouquet, F.-X. Felpin, J. Organomet. Chem. 755 (2014) 78-85.
[34] S.K. Bharadwaj, P.K. Boruah, P.K. Gogoi, Catal. Commun. 57 (2014) 124-128.
[35] SMART, Bruker AXS (2000).
[36] G.M. Sheldrick, Acta. Cryst. A46 (1990) 467-473.
[37] G.M. Sheldrick, SHELXL-97, Universitat Gottingen (1997).
[38] A.L. Spek, Platon - A Multipurpose Crystallographic Tool Utrecht, Utrecht University, The Netherlands (2005).
[39] M. Feng, F. Pointillart, B. Lefeuvre, V. Dorcet, S. Golhen, O. Cador, L. Ouahab, Inorg.

Chem. 54 (2015) 4021-4028.
[40] M. Feng, S. Speed, F. Pointillart, B. Lefeuvre, B. Le Guennic, S. Golhen, O. Cador, L. Ouahab, Eur. J. Inorg. Chem. 2016 (2016) 2039-2050.
[41] J.-H. Zou, D.-L. Zhu, F.-F. Li, F.-S. Li, H. Wu, Q.-Y. Li, G.-W. Yang, P. Zhang, Y.-X. Miao, J. Xie, Z. Anorg. Allg. Chem. 640 (2014) 2226-2231.
[42] M. Yawer, M. Kariem, P. Sood, H.N. Sheikh, CrystEngComm, 18 (2016).
a) V.A. Blatov, A.P. Shevchenko, D.M. Proserpio, Cryst. Growth Des. 14 (2014) 3576-3586.
[43] H. Zhao, S.-Y. Zhou, C. Feng, N.-X. Wei, G.-G. Wang, Inorg. Chim. Acta 421 (2014) 169-175.
[44] M.S.M. Abdelbaky, Z. Amghouz, E. Fernández-Zapico, S. García-Granda, J.R. García, J. Solid State Chem. 229 (2015) 197-207.
[45] A. Ostasz, R. Łyszczek, L. Mazur, J. Sienkiewicz-Gromiuk, I. Rusinek, Z. Rzączyńska, J. Anal. Appl. Pyrol. 99 (2013) 203-210.
[46] S.-M. Fang, E.C. Sañudo, M. Hu, Q. Zhang, S.-T. Ma, L.-R. Jia, C. Wang, J.-Y. Tang, M. Du, C.-S. Liu, Cryst. Growth Des. 11 (2011) 811-819.
[47] L. Zhang, N. Yu, K. Zhang, R. Qiu, Y. Zhao, W. Rong, H. Deng, Inorg. Chim. Acta 400 (2013) 67-73.
[48] J. Feng, J.-B. Yu, S.-Y. Song, L.-N. Sun, W.-Q. Fan, X.-M. Guo, S. Dang, H.-J. Zhang, Dalton T. (2009) 2406.
[49] Y.-X. Chi, S.-Y. Niu, J. Jin, Inorg. Chim. Acta 362 (2009) 3821-3828.
[50] J. Feng, L. Zhou, S.-Y. Song, Z.-F. Li, W.-Q. Fan, L.-N. Sun, Y.-N. Yu, H.-J. Zhang, Dalton T. (2009) 6593.
[51] X. Li, Y.-B. Zhang, Y.-Q. Zou, J. Mol. Struct. 919 (2009) 277-283.
[52] M. Filipescu, N. Scarisoreanu, V. Craciun, B. Mitu, A. Purice, A. Moldovan, V. Ion, O. Toma, M. Dinescu, Appl. Surf. Sci. 253 (2007) 8184-8191.
[53] B. Ay, N. Doğan, E. Yildiz, İ. Kani, Polyhedron, 88 (2015) 176-181.
[54] H. Xie, G. Lu, J. Rare Earth. 31 (2013) 639-644.
[55] Q.-B. Bo, J.-J. Pang, H.-Y. Wang, C.-H. Fan, Z.-W. Zhang, Inorg. Chim. Acta 428 (2015) 170-175.
[56] Y.-S. Song, B. Yan, Z.-X. Chen, J. Mol. Struct. 750 (2005) 101-108.
[57] B. Ay, E. Yildiz, A.C. Felts, K.A. Abboud, J. Solid State Chem. 244 (2016) 61-68.

Graphical Abstract (Synopsis)

Two novel 3D lanthanide-organic frameworks have been synthesized under hydrothermal conditions. The catalytic performances of MOFs were investigated and their selectivities were measured as 100% for the oxidation of thymol to thymoquinone. The photoluminescence properties of the MOFs have also been examined.

Graphical Abstract (Pictogram)